Quantum path interference in the wavelength-dependent below-threshold harmonic generation

Lixin He,[1] Pengfei Lan,[1,2,*] Chunyang Zhai,[1] Yang Li,[1] Zhe Wang,[1] Qingbin Zhang,[1,2] and Peixiang Lu[1,2,†]

[1]*School of Physics and Wuhan National Laboratory for Optoelectronics, Huazhong University of Science and Technology, Wuhan 430074, China*

[2]*Key Laboratory of Fundamental Physical Quantities Measurement of Ministry of Education, Wuhan 430074, China*

(Received 15 December 2014; published 24 February 2015)

We have theoretically investigated the wavelength-dependent below-threshold harmonic (BTH) generation in different laser intensity regimes. Based on the simulations of the time-dependent Schrödinger equation, we find a periodic fluctuation in the wavelength-dependent BTH yields with laser intensities in the magnitude of 10^{13} W/cm^2. This result shows significant differences from the resonance peak structures in the recent study with intensities about 10^{12} W/cm^2 [Xiong *et al.*, Phys. Rev. Lett. **112**, 233001 (2014)]. By performing both the quantum path analysis and time-frequency transform of the harmonic spectra, we demonstrate that the difference in the wavelength-dependent BTH yields is due to the complicated quantum path distributions of BTHs with the intensities in the magnitude of 10^{13} W/cm^2. And the periodic fluctuation is further demonstrated to originate from the interference between the two quantum paths that dominate the harmonic generation.

DOI: 10.1103/PhysRevA.91.023428 PACS number(s): 32.80.Qk, 33.80.Wz, 32.80.Wr, 42.50.Hz

I. INTRODUCTION

When intense laser pulses interact with atoms or molecules, high-order-harmonic generation (HHG) will occur [1]. Nowadays, HHG has been the most effective approach to produce attosecond extreme ultraviolet pulses [2–10], which can serve as an important tool for probing the ultrafast electronic dynamics inside atoms or molecules [11–16], and inaugurating a new domain for time-resolved metrology on the attosecond time scale [17]. During the laser-molecular interaction, the generated harmonics also provide an effective way for the tomographic imaging of molecular orbital [18–23]. Due to its potential applications, the HHG has attracted much attention in the past several decades.

The observed harmonic spectrum has a characteristic shape: it falls off at the first few harmonics then exhibits a plateau where all the harmonics have the comparable strength, and ends up with a sharp cutoff. In most previous studies, investigators mainly pay their attention to the harmonics generated in the plateau region, i.e., the above-threshold harmonics (ATHs). For ATH generation, the underlying process can be qualitatively explained in terms of the semiclassical model (SCM) [24]. In this model harmonics are produced in three steps: (i) ionization, (ii) acceleration, and (iii) recombination. During the recombination, the electron will release its kinetic energy in the form of high-order-harmonic emission. The energy of the emitted photon is then given by $\Omega = E_k + I_p$, where I_p is the ionization potential and E_k is the electronic kinetic energy gained in the laser field. The SCM has been used to well understand the observed high harmonic cutoff $I_p + 3.17U_p$. Here $U_p = I/4\omega^2$ is the ponderomotive energy, and I and ω are the laser intensity and frequency, respectively. For a quantum-mechanical version of the SCM, Lewenstein *et al.* [25] have developed a strong-field approximation (SFA) model to quantitatively describe the HHG process. The SFA has predicted many fundamental characteristics of HHG, in particular, the fact that for each harmonic below the cutoff, there are two electronic pathways, which are commonly referred to as the short and long quantum paths [26], contributing to the harmonic generation. According to SFA, the phase acquired by the electron wave function along each path is proportional to the cycle-averaged intensity and is in general different for the short and long paths [26–28]. This gives rise to an interference effect in the intensity-dependent HHG yield, as has been observed in Refs. [29,30]. Nevertheless, in the conventional SCM SFA, the effect of Coulomb potential is ignored in the acceleration step and the lowest possible value of E_k is zero. Therefore, the standard SCM or SFA is not applicable to describe the generation of harmonics below the ionization threshold.

Recently, the generation of below-threshold harmonics (BTHs) has attracted much attention from investigators and several works about BTHs have been carried out. In particular, Yost *et al.* [30] have investigated the BTH generation in xenon atoms by using a 1.07 μm driving laser field. In their experiment, they observe that the harmonic yield can increase stepwise with increasing the driving laser intensity. This result has been demonstrated to result from the interference between two distinct quantum paths with different intensity-dependent phases. The experimental observations were further supported by Hostetter *et al.* [31] from a generalized SCM of harmonic generation, in which the atomic Coulomb potential is included. Apart from the quantum path theory, an alternative way to understand the BTH is based on the resonance theory [32–34]. Recently, Michael Chini *et al.* [33] found that the ninth harmonic (H9, near the ionization threshold) exhibits narrow-linewidth spectral enhancements in the vicinity of the atomic resonances. In addition, Xiong *et al.* [34] have also proposed two resonance mechanisms in both the photon absorption and photon emission steps to explain the behavior of the wavelength-dependent BTH. However, in their work, the laser intensity is confined to the magnitude of 10^{12} W/cm^2.

In this paper, we have investigated the wavelength-dependent BTH generation with the laser intensities in the magnitude of 10^{13} W/cm^2. The calculated result shows a periodic fluctuation in the wavelength-dependent BTH yields,

*pengfeilan@mail.hust.edu.cn
†lupeixiang@mail.hust.edu.cn

which is different from the resonance peak structures with lower intensities ($\sim 10^{12}$ W/cm^2) in Ref. [34]. This difference can no longer be well understood in terms of the resonance theory, since the resonant two states can remain roughly stable as the laser intensity is increased [34]. Furthermore, by performing the quantum path analysis and the time-frequency transform of the harmonic spectrum, we have successfully explained the origin of the different behaviors in the wavelength-dependent BTH yields according to the quantum path distributions of BTHs. In addition, we have also demonstrated that the fluctuation in the wavelength-dependent BTH yields with higher intensities mainly results from the interference of two quantum paths characterized by different phase coefficients. Note that the fluctuation phenomenon has also been observed in the yield of the ionization rate [35]. However, in that case, the laser intensity is about 10^{14-16} W/cm^2, and the fluctuation structures mainly result from the suppression-of-ionization effect.

II. THEORETICAL MODEL

The interaction of atoms with an intense laser field can be accurately modeled by solving the time-dependent Schrödinger equation (TDSE) in three spatial dimension,

$$i\frac{\partial \Psi(\mathbf{r},t)}{\partial t} = H(t)\Psi(\mathbf{r},t) = \left[-\frac{1}{2}\nabla^2 + V_{\text{atom}}(r) + V_l(\mathbf{r},t)\right]\Psi(\mathbf{r},t), \quad (1)$$

where $V_{\text{atom}}(r)$ is the Coulomb potential of the atom. In our simulations, we choose hydrogen as the target atom, of which the ionization threshold is about 13.6 eV, and the corresponding atomic potential has the form of $V_{\text{atom}}(r) = -1/r$. The potential $V_l(\mathbf{r},t) = \mathbf{r}\cdot\mathbf{E}(t)$ represents the interaction term of the atomic electron and the laser field. We assume that the laser field is linearly polarized along the z axis. Then the potential $V_l(\mathbf{r},t)$ can be expressed as

$$V_l(\mathbf{r},t) = \mathbf{r}\cdot\mathbf{E}(t) = E_0 z f(t)\cos(\omega t + \phi). \quad (2)$$

Here, E_0 is the amplitude, ω is the frequency, and ϕ is the carrier-envelope phase (CEP) of the incident laser pulse. Unless otherwise stated, the ϕ is set to zero. $f(t)$ is the envelope of the laser field. In our investigation, the incident laser field is selected with a sin-squared envelope, and the duration of the laser pulse is fixed at 20 optical cycles for each laser wavelength. Equation (1) can be effectively solved in the spherical polar coordinates by using the well-known split-operator method [36]. To avoid the reflections from the spatial boundaries, the electron wave function is multiplied by a mask function of the form $\cos^{1/8}$ at each time step. Once the electron wave function $\Psi(r,t)$ is obtained, the time-dependent dipole acceleration can be calculated by means of

$$a(t) = \frac{d^2\langle r\rangle}{dt^2} = -\langle\Psi(t)|[H(t),[H(t),z]]|\Psi(t)\rangle, \quad (3)$$

where $H(t)$ is the Hamiltonian of the electron in the laser field. Then, the harmonic spectrum is obtained by Fourier transforming the dipole acceleration $a(t)$:

$$a_q = \left|\frac{1}{T}\int_0^T a(t)\exp(-iq\omega t)\right|^2, \quad (4)$$

where T is the duration of the laser pulse and q corresponds to the harmonic order.

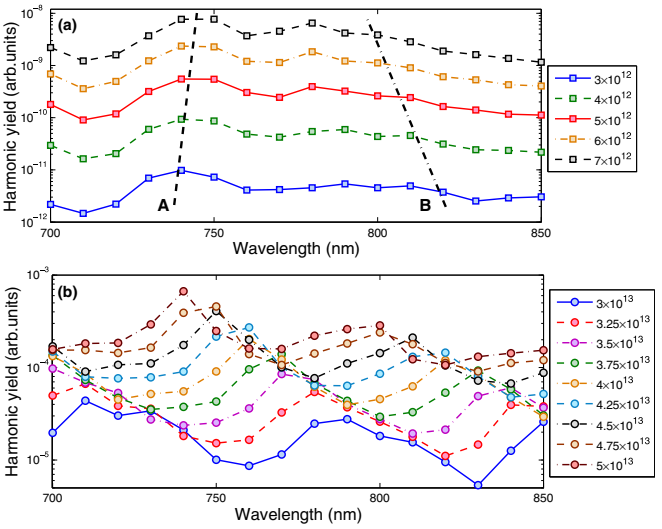

FIG. 1. (Color online) (a) Wavelength dependence of the integrated harmonic yield for the ninth harmonic (H9) with the laser intensity varying from 3×10^{12} W/cm^2 to 7×10^{12} W/cm^2 (from bottom to top). (b) Same as (a), but for some higher laser intensities that vary from 3×10^{13} W/cm^2 to 5×10^{13} W/cm^2 (from bottom to top).

III. RESULTS AND DISCUSSION

In Fig. 1(a), we have first calculated the wavelength-dependent (from 700 nm to 850 nm) HHG yields for the ninth harmonic (H9) with the laser intensity changing from 3×10^{12} W/cm^2 to 7×10^{12} W/cm^2 (from bottom to top). Here, the harmonic yield is integrated within one photon energy range and our calculated results show a good agreement with that in Ref. [34]. To be specific, at the laser wavelength near 740 nm, it exhibits a distinct peak structure [marked as A (dashed line)] in the wavelength-dependent yields of H9. And the peak A can remain roughly stable as the laser intensity increases. Whereas in the wavelength range of 800–820 nm, where the photon energy of H9 is near the ionization threshold, an alleged peak B (marked as dash-dotted line) is extremely broadened and one can barely observe a clear peak structure. To explain the above phenomenon, Xiong *et al.* [34] have presented two resonance mechanisms, i.e., the "resonance absorption" and "resonance emission." According to their opinions, the peak A mainly originates from the enhancement of HHG yield related to a multiphoton resonance absorption between low-lying excited states with respect to the ground state. And the disappearance of peak B is caused by the resonance of electrons in the recombination step, which only occurs when the harmonic energy is near the ionization threshold. They suppose that for harmonics with photon energy near ionization threshold, the return electrons can be trapped

in the high-lying Rydberg states for a long time and obtain an additional phase, which will further influence the quantum path interference and eventually leads to disappearance of the interference peak B. However, in Fig. 1(b), we have also calculated the wavelength-dependent HHG yield of H9 with much higher laser intensities (from 3×10^{13} W/cm^2 to 5×10^{13} W/cm^2). The calculated results are quite different from that in Fig. 1(a). As shown in Fig. 1(b), with the higher laser intensities, it displays a periodical fluctuation in the wavelength-dependent HHG yields, rather than the marked resonance peaks A and B with lower ones in Fig. 1(a). This significant difference can no longer be explained with the resonance theory, since the resonant two states are relatively stable against the change of the laser intensity [34].

To clarify the different behaviors in the wavelength-dependent BTH yields mentioned above, we next perform the quantum path analysis for BTH generation. Even though the generation of BTH cannot be accurately estimated by the conventional SFA, the concept of quantum paths in SFA can still be generalized to understand this phenomenon. To associate our full quantum mechanical TDSE calculations with the semiclassical picture, we have analyzed the intensity-dependent dipole moment $d_q(I)$ for each harmonic q in terms of its conjugate variable α (for details, see Refs. [31,37]),

$$D_q(\alpha, I_0) = \int d_q(I)\exp(i\alpha q)W(I - I_0)dI. \qquad (5)$$

Here $W(I - I_0)$ is a translating window function centered at I_0, and $D_q(\alpha, I_0)$ represents the contribution from the phase component α over a range of intensities around I_0. For each phase component α, it corresponds to a quantum path of electrons in the semiclassical picture, and the size of α is an approximate measure of the traveling time of electrons in the continuum [25]. The evolution phase of electron wave packet from the quantum path characterized by phase coefficient α is then given by $S = -\alpha U_p/\omega$ [38]. For the generation of ATH, the phase coefficients obtained from the full quantum calculations have been demonstrated to agree well with the prediction of SCM. In particular, the short and long quantum paths correspond to phase coefficients $\alpha_1 \approx 0.1-0.2\pi$ and $\alpha_2 \approx 2\pi$, respectively.

In Fig. 2, we have applied the above quantum path analysis to the generation of BTHs. Figure 2(a) shows the calculated quantum path distributions (QPDs) for H9 driven by an 810 nm laser field with the intensity changing from 3×10^{13} W/cm^2 to 7×10^{13} W/cm^2. We find that the distributions are complicated. For each laser intensity, there are more than one quantum paths, characterized by different phase coefficients α, contributing to the harmonic generation. To obtain a clear insight, we have investigated the detail QPDs for H9 with the laser intensity centered at 4×10^{13} W/cm^2, 5×10^{13} W/cm^2, and 6×10^{13} W/cm^2. Corresponding results are presented in Figs. 2(c)–2(e), respectively. One can clearly see that, in each panel, the spectrum is dominated by two peaks that correspond to the phase coefficients $\alpha_1 \approx 0$ and $\alpha_2 \approx 3\pi$. This result agrees well with that mentioned in Refs. [30,31]. In addition, we can also see the contributions from some smaller peaks with larger α values, for instance, $\alpha \approx 4\pi$ and $\alpha \approx 7\pi$. For these paths, electrons suffer longer traveling time in the continuum. Due to the quantum diffusion, these paths have

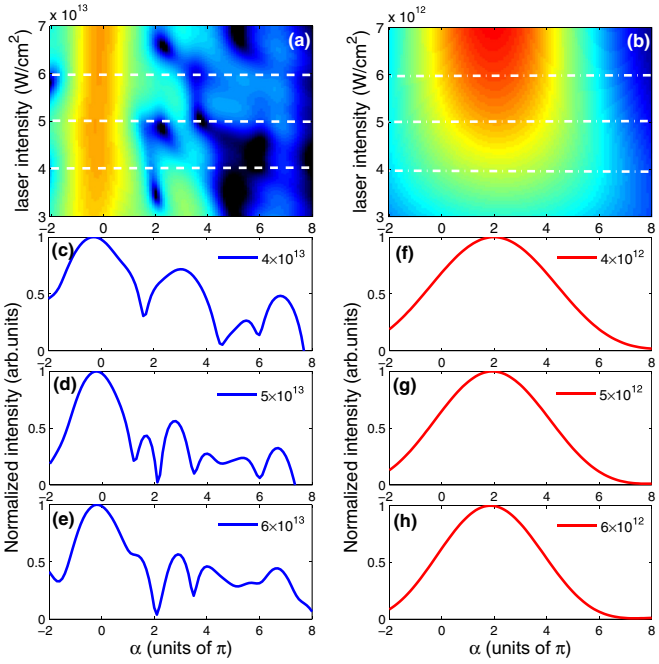

FIG. 2. (Color online) (a) Quantum path distribution for H9 driven by a 810 nm laser field with the intensity varying from 3×10^{13} W/cm^2 to 7×10^{13} W/cm^2. (b) Same as (a), but for the laser intensity varying from 3×10^{12} W/cm^2 to 7×10^{12} W/cm^2. (c)–(h) Quantum path distributions for H9 at six specific laser intensities [corresponding to the transverse lines in (a) and (b)]: (c) 4×10^{13} W/cm^2, (d) 5×10^{13} W/cm^2, (e) 6×10^{13} W/cm^2, (f) 4×10^{12} W/cm^2, (g) 5×10^{12} W/cm^2, and (h) 6×10^{12} W/cm^2.

much smaller amplitudes, as is shown here. For comparison, we have also performed quantum path analysis for H9 with some lower intensities that vary from 3×10^{12} W/cm^2 to 7×10^{12} W/cm^2. As shown in Fig. 2(b), with lower laser intensities, the QPDs are mainly concentrated in the area where α is close to 2π. Clear insights can also be found in Figs. 2(f)–2(h), which show the QPDs for the intensity of 4×10^{12} W/cm^2, 5×10^{12} W/cm^2, and 6×10^{12} W/cm^2, respectively. It is obvious that in each panel, only one broad peak centered at $\alpha \approx 2\pi$ exists, which means that the emission of H9 is mainly along the quantum path characterized by $\alpha \approx 2\pi$.

To obtain a better understanding of the origin of the QPDs in Fig. 2, we have performed the time-frequency analysis for the BTHs generated in an 810 nm laser field. Calculation details can be found in Ref. [39] and the references therein. Figures 3(a) and 3(b) are the results for the intensity of 4×10^{13} W/cm^2 and 4×10^{12} W/cm^2, respectively. As shown in Fig. 3(a), for the generation of H9, it displays a netlike structure in the time-frequency spectrum, which consists of a longitudinal distribution A (marked as the blue solid line) and a transverse distribution B (marked as the black dashed line). For the transverse distribution B, the pattern is very similar to that for the ATH. Corresponding electronic dynamics process can be described by using the generalized SCM [30,31], in which the atomic potential is present. Due to the influence of the atomic potential, the harmonic emission is limited to follow the generalized long quantum path, of which the

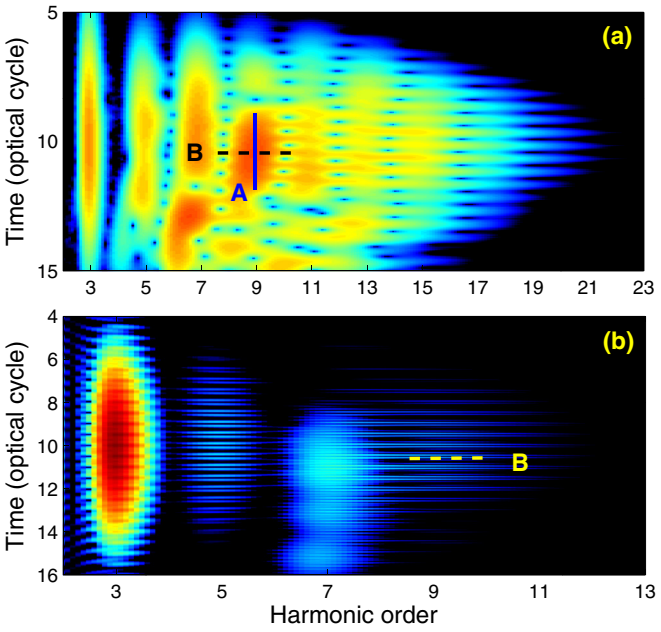

FIG. 3. (Color online) (a) Time-frequency distribution for the harmonics generated in an 810 nm laser field with the intensity of 4×10^{13} W/cm^2. (b) Same as (a), but for the intensity of 4×10^{12} W/cm^2.

electron wave packet accumulates a larger intensity-dependent phase than that with $\alpha \approx 2\pi$ for ATH. In Fig. 2(c) (QPDs for H9 at 4×10^{13} W/cm^2), the quantum path characterized by $\alpha \approx 3\pi$ mainly originates from the transverse distribution B. Whereas for the longitudinal distribution A, the harmonic emission is continuous in the time domain and for the qth harmonic, the corresponding time profile of A resembles the envelope of $I^q(t)$ [40]. Here $I(t)$ is the time-dependent laser intensity. This feature can be associated with a multiphoton process, which has no intensity-dependent phase and will further lead to the quantum path characterized by $\alpha \approx 0$, as shown in Fig. 2(c). For the quantum paths with larger values of α in Fig. 2(c), they are mainly attributed to high-order rescattering events, as reported in Refs. [41,42]. However, in Fig. 3(b), we find that only the transverse distribution B makes contributions to the generation of H9. That is why we did not find the quantum path with $\alpha \approx 0$ in Fig. 2(f) (QPDs for H9 at 4×10^{12} W/cm^2). Besides, we also note that, with the intensity of 4×10^{12} W/cm^2, the H9 is very close to the cutoff range. So the obtained phase coefficient [$\alpha \approx 2\pi$ in Fig. 2(f)] is somewhat smaller than that in the plateau range ($\alpha \approx 3\pi$ for BTH).

Based on the calculated QPDs in Fig. 2, we can then explain the different behaviors in the wavelength-dependent BTH yields in Fig. 1 by using the quantum path theory. To be specific, for the cases of the intensity in the magnitude of 10^{12} W/cm^2, only one prominent quantum path with the $\alpha \approx 2\pi$ [see Fig. 1(b)] contributes to the BTH generation, and no obvious interference phenomenon will occur in the HHG process. Therefore, we cannot find a distinct fluctuation in the wavelength-dependent BTH yields [as shown in Fig. 1(a)]. For the cases of the intensity in the magnitude of 10^{13} W/cm^2, the BTH generation is primarily dominated by the two

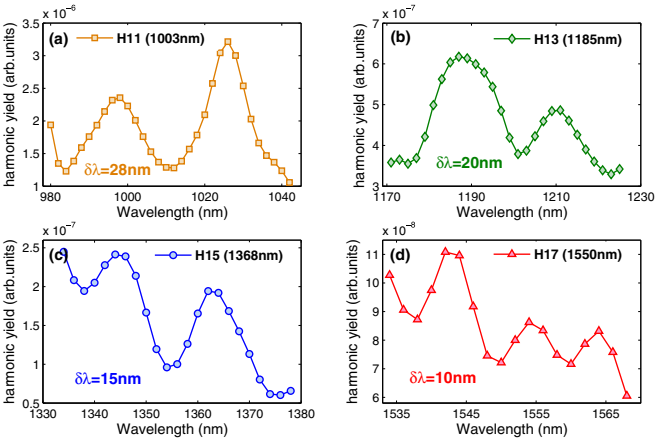

FIG. 4. (Color online) (a) Variations of the integrated harmonic yield for H11 in a narrow wavelength range around 1003 nm. (b)–(d) Same as (a), but for H13 around 1185 nm, H15 around 1368 nm, and H17 around 1550 nm, respectively. Here, the laser intensity is chosen as 3×10^{13} W/cm^2. In each panel, the integrated harmonic has the photon energy close to I_p (ionization threshold of hydrogen atom, 13.6 eV).

quantum paths characterized by $\alpha_1 \approx 0$ and $\alpha_2 \approx 3\pi$. The phase difference between the two paths is then expressed as $S_{12} = (\alpha_2 - \alpha_1)U_p/\omega$, which is proportional to $I\lambda^3$. At a constant laser intensity, with the S_{12} changed by 2π, it will precisely give rise to a periodic fluctuation in the wavelength-dependent HHG yields [as can be seen in Fig. 1(b)]. The corresponding period of the fluctuation can be evaluated by

$$\delta S_{12} = \frac{dS_{12}}{d\lambda}\delta\lambda = 2\pi, \tag{6}$$

namely,

$$\delta\lambda \propto \lambda^{-2}. \tag{7}$$

To confirm our above interpretation, we have calculated the wavelength-dependent BTH yields at some longer driving wavelengths with the intensity of 3×10^{13} W/cm^2. Figures 4(a)–4(d) present the corresponding results for the eleventh harmonic (H11) near 1003 nm, thirteenth harmonic (H13) near 1185 nm, fifteenth harmonic (H15) near 1368 nm, and seventeenth harmonic (H17) near 1550 nm, respectively. It is worth mentioning that, in Fig. 4, all the integrated harmonics have the photon energy near the ionization threshold. If the resonance mechanism mentioned in Ref. [34] works here, the calculated results should be similar to that in Fig. 1(a) and one can barely find a fluctuation in the wavelength-dependent HHG yields. However, the fact is opposite. In each panel, we have discovered a periodic fluctuation in the wavelength-dependent HHG yields. For the driving wavelength of 1003 nm, 1185 nm, 1368 nm, and 1550 nm, the corresponding periods $\delta\lambda$ are 28 nm, 20 nm, 15 nm, and 10 nm, respectively. We have also presented the period of the fluctuation as a function of the driving laser wavelength. Corresponding result is shown in Fig. 5. The period is demonstrated to scale approximately as $\lambda^{-2.4}$, which is very close to the prediction of the quantum path theory. This result indicates that the fluctuation in the

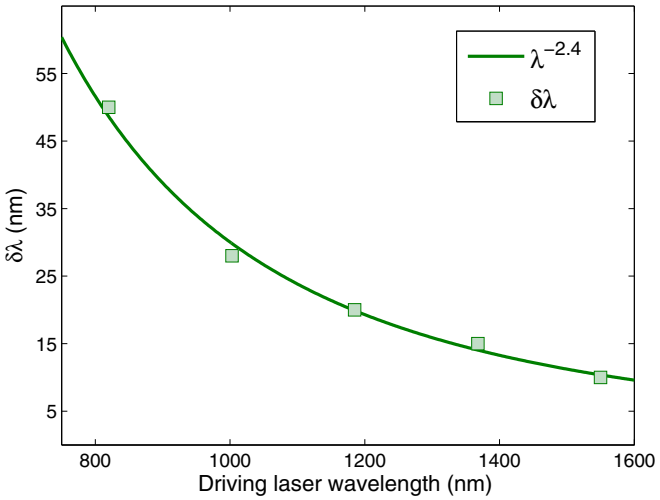

FIG. 5. (Color online) Modulation period $\delta\lambda$ as a function of the driving laser wavelength with the laser intensity of 3×10^{13} W/cm^2.

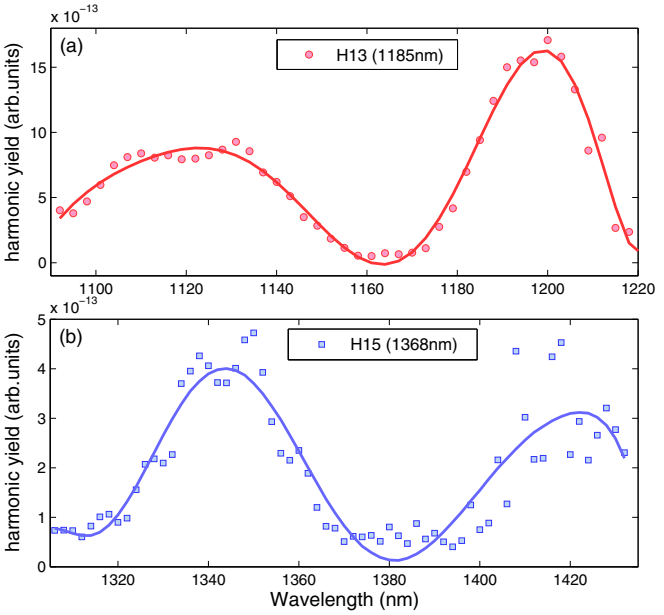

FIG. 6. (Color online) (a),(b) Same as Figs. 4(b) and 4(c), respectively, but for a lower driving laser intensity of 6×10^{12} W/cm^2.

wavelength-dependent BTH yields indeed originates from the quantum path interference.

Finally, we have also investigated the BTH generation at longer wavelengths with a lower laser intensity of 6×10^{12} W/cm^2. Figures 6(a) and 6(b) show the wavelength-dependent HHG yields for H13 near 1185 nm, and H15 near 1368 nm, respectively. One can see pronounced fluctuations exist in the wavelength-dependent HHG yields. This result is mainly attributed to the cutoff extension by using longer laser wavelengths. In Figs. 6(a) and 6(b), the H13 and H15 locate far from the cutoff range, and both the longitudinal distribution A and transverse distribution B contribute to the harmonic generation, which will consequently lead to the interference phenomenon, i.e., the fluctuation structure in the wavelength-dependent HHG yields.

IV. CONCLUSION

In conclusion, we have investigated the wavelength-dependent BTH generation driven by using laser pulses with different intensities. Based on our numerical solutions of TDSE, we find that with the laser intensity in the magnitude of 10^{13} W/cm^2, it exhibits a periodic fluctuation in the wavelength-dependent BTH yields, whereas this phenomenon is not discovered with the intensity in the magnitude of 10^{12} W/cm^2. By preforming the quantum path analysis and the time-frequency transform for BTHs, we find that, with the intensities in the magnitude of 10^{13} W/cm^2, there are two dominated quantum paths characterized by $\alpha \approx 0$ and $\alpha \approx 3\pi$ contributing to the BTH generation. The interference between the two quantum paths just gives rise to the fluctuation in the wavelength-dependent HHG yields, while for the cases of the intensities in the magnitude of 10^{12} W/cm^2, we demonstrate that only one quantum path with $\alpha \approx 2\pi$ contributes to BTH. Consequently, one cannot observe an interference phenomenon in the wavelength-dependent HHG yields. In addition, we also note that, by increasing the laser wavelength, the interference phenomenon can also be observed with the laser intensities in the magnitude of 10^{12} W/cm^2.

ACKNOWLEDGMENTS

This work was supported by the 973 Program of China under Grant No. 2011CB808103 and the National Natural Science Foundation of China under Grants No. 61275126, No. 11234004, and No. 11204095. Numerical simulations presented in this paper were carried out using the High Performance Computing experimental testbed in SCTS/CGCL.

[1] A. McPherson *et al.*, J. Opt. Soc. Am. B **4**, 595 (1987); M. Ferray *et al.*, J. Phys. B **21**, L31 (1988).

[2] I. P. Christov, M. M. Murnane, and H. C. Kapteyn, Phys. Rev. Lett. **78**, 1251 (1997).

[3] P. M. Paul, E. S. Toma, P. Breger, G. Mullot, F. Aug, Ph. Balcou, H. G. Muller, and P. Agostini, Science **292**, 1689 (2001).

[4] Y. Mairesse *et al.*, Science **302**, 1540 (2003).

[5] W. Cao, P. Lu, P. Lan, X. Wang, and G. Yang, Phys. Rev. A **74**, 063821 (2006); P. Lan, P. Lu, W. Cao, Y. Li, and X. Wang, *ibid.* **76**, 051801 (2007).

[6] E. Goulielmakis, M. Schultze, M. Hofstetter, V. S. Yakovlev, J. Gagnon, M. Uiberacker, A. L. Aquila, E. M. Gullikson, D. T. Attwood, R. Kienberger, F. Krausz, and U. Kleineberg, Science **320**, 1614 (2008).

[7] P. Lan, P. Lu, W. Cao, Y. Li, and X. Wang, Phys. Rev. A **76**, 011402(R) (2007); P. Lan, P. Lu, W. Cao, and X. Wang, *ibid.* **76**, 043808 (2007); W. Cao, P. Lu, P. Lan, X. Wang, and G. Yang, Opt. Express **15**, 530 (2007).

[8] E. J. Takahashi, T. Kanai, K. L. Ishikawa, Y. Nabekawa, and K. Midorikawa, Phys. Rev. Lett. **101**, 253901 (2008);

E. J. Takahashi, P. Lan, O. D. Mücke, Y. Nabekawa, and K. Midorikawa, *ibid.* **104**, 233901 (2010).
[9] K. Zhao, Q. Zhang, M. Chini, Y. Wu, X. Wang, and Z. Chang, Opt. Lett. **37**, 3891 (2012).
[10] J. Luo, Y. Li, Z. Wang, Q. Zhang, and P. Lu, J. Phys. B **46**, 145602 (2013).
[11] R. Kienberger *et al.*, Science **297**, 1144 (2002).
[12] M. Uiberacker *et al.*, Nature (London) **446**, 627 (2007).
[13] Y. Zhou, C. Huang, Q. Liao, and P. Lu, Phys. Rev. Lett. **109**, 053004 (2012).
[14] L. Zhang *et al.*, Phys. Rev. Lett. **112**, 193002 (2014).
[15] Q. Liao, Y. Zhou, C. Huang, and P. Lu, New J. Phys. **14**, 013001 (2012); C. Huang, Y. Zhou, Q. Zhang, and P. Lu, Opt. Express **21**, 11382 (2013).
[16] C. Huang, P. Lan, Y. Zhou, Q. Zhang, K. Liu, and P. Lu, Phys. Rev. A **90**, 043420 (2014).
[17] M. Drescher, M. Hentschel, R. Kienberger, M. Uiberacker, V. Yakovelv, A. Scrinzi, Th. Westerwalbesloh, U. Kleineberg, U. Heinzmann, and F. Krausz, Nature (London) **419**, 803 (2002).
[18] J. Itatani, J. Levesque, D. Zeidler, H. Niikura, H. Ppin, J. C. Kieffer, P. B. Corkum, and D. M. Villeneuve, Nature (London) **432**, 867 (2004).
[19] M. Lein, J. Phys. B **40**, R135 (2007).
[20] M. Qin, X. Zhu, Q. Zhang, and P. Lu, Opt. Lett. **37**, 5208 (2012).
[21] E. V. van der Zwan and M. Lein, Phys. Rev. Lett. **108**, 043004 (2012).
[22] X. Zhu, M. Qin, Y. Li, Q. Zhang, Z. Xu, and P. Lu, Phys. Rev. A **87**, 045402 (2013).
[23] Y. Li, X. Zhu, P. Lan, Q. Zhang, M. Qin, and P. Lu, Phys. Rev. A **89**, 045401 (2014).
[24] P. B. Corkum, Phys. Rev. Lett. **71**, 1994 (1993).
[25] M. Lewenstein, Ph. Balcou, M. Yu. Ivanov, A. L'Huillier, and P. B. Corkum, Phys. Rev. A **49**, 2117 (1994).
[26] P. Antoine, A. L'Huillier, and M. Lewenstein, Phys. Rev. Lett. **77**, 1234 (1996).
[27] M. Bellini, C. Lyngå, A. Tozzi, M. B. Gaarde, T. W. Hänsch, A. L'Huillier, and C.-G. Wahlström, Phys. Rev. Lett. **81**, 297 (1998).
[28] S. Kazamias and Ph. Balcou, Phys. Rev. A **69**, 063416 (2004).
[29] A. Zaïr *et al.*, Phys. Rev. Lett. **100**, 143902 (2008).
[30] D. C. Yost, T. R. Schibli, J. Ye, J. L. Tate, J. Hostetter, M. B. Gaarde, and K. J. Schafer, Nat. Phys. **5**, 815 (2009).
[31] J. A. Hostetter, J. L. Tate, K. J. Schafer, and M. B. Gaarde, Phys. Rev. A **82**, 023401 (2010).
[32] Ph. Balcou and A. L'Huillier, Phys. Rev. A **47**, 1447 (1993).
[33] M. Chini, X. Wang, Y. Cheng, H. Wang, Y. Wu, E. Cunningham, P. Li, J. Heslar, D. A. Telnov, S.-I. Chu, and Z. Chang, Nat. Photon. **8**, 381 (2014).
[34] W.-H. Xiong, J.-W. Geng, J.-Y. Tang, L.-Y. Peng, and Q. Gong, Phys. Rev. Lett. **112**, 233001 (2014).
[35] G. Yao and S.-I. Chu, Phys. Rev. A **45**, 6735 (1992).
[36] M. R. Hermann and J. A. Fleck, Jr., Phys. Rev. A **38**, 6000 (1988).
[37] Ph. Balcou, A. S. Dederichs, M. B. Gaarde, and A. L'Huillier, J. Phys. B **32**, 2973 (1999).
[38] M. B. Gaarde and K. J. Schafer, Phys. Rev. A **65**, 031406(R) (2002).
[39] Q. Zhang, P. Lu, W. Hong, Q. Liao, P. Lan, and X. Wang, Phys. Rev. A **79**, 053406 (2009).
[40] K. Nasiri Avanaki, D. A. Telnov, and S.-I. Chu, Phys. Rev. A **90**, 033425 (2014).
[41] P.-C. Li, Y.-L. Sheu, C. Laughlin, and S.-I. Chu, Phys. Rev. A **90**, 041401(R) (2014).
[42] L. He, Y. Li, Z. Wang, Q. Zhang, P. Lan, and P. Lu, Phys. Rev. A **89**, 053417 (2014).